PLOS ONE

RESEARCH ARTICLE

Calculated thickness dependent plasmonic properties of gold nanobars in the visible to near-infrared light regime

Pijush K. Ghosh[1,2], Desalegn T. Debu[1], David A. French[1], Joseph B. Herzog[1]*

1 Department of Physics, University of Arkansas, Fayetteville, Arkansas, United States of America, **2** Department of Electrical Engineering, University of Arkansas, Fayetteville, Arkansas, United States of America

* jbherzog@uark.edu

Citation: Ghosh PK, Debu DT, French DA, Herzog JB (2017) Calculated thickness dependent plasmonic properties of gold nanobars in the visible to near-infrared light regime. PLoS ONE 12 (5): e0177463. https://doi.org/10.1371/journal.pone.0177463

Editor: Yogendra Kumar Mishra, Institute of Materials Science, GERMANY

Received: December 24, 2016

Accepted: April 27, 2017

Published: May 9, 2017

Data Availability Statement: All relevant data are within the paper and its Supporting Information files.

Funding: Support was provided by Arkansas Biosciences Institute, the major research component of the Arkansas Tobacco Settlement Proceeds Act of 2000 [http://arbiosciences.org]. The funders had no role in study design, data collection and analysis, decision to publish, or preparation of the manuscript.

Abstract

Metallic, especially gold, nanostructures exhibit plasmonic behavior in the visible to near-infrared light range. In this study, we investigate optical enhancement and absorption of gold nanobars with different thicknesses for transverse and longitudinal polarizations using finite element method simulations. This study also reports on the discrepancy in the resonance wavelengths and optical enhancement of the sharp-corner and round-corner nanobars of constant length 100 nm and width 60 nm. The result shows that resonance amplitude and wavelength have strong dependences on the thickness of the nanostructure as well as the sharpness of the corners, which is significant since actual fabricated structure often have rounded corners. Primary resonance mode blue-shifts and broadens as the thickess increases due to decoupling of charge dipoles at the surface for both polarizations. The broadening effect is characterized by measuring the full width at half maximum of the spectra. We also present the surface charge distribution showing dipole mode oscillations at resonance frequency and multimode resonance indicating different oscillation directions of the surface charge based on the polarization direction of the field. Results of this work give insight for precisely tuning nanobar structures for sensing and other enhanced optical applications.

Introduction

When light illuminates metal nanostructures, the free electron gas density oscillates collectively. This collective oscillation is known as a *surface plasmon* or simply a *plasmon*. Strong local-field enhancements, light absorption, and scattering all occur at a resonant incident wavelength, which can depend on the polarization of the light [1–3]. Due to their small volume, gold nanobars exhibit little radiation damping [1]; as a result, they show large local-field enhancement factors and large light scattering efficiency. Because of these characteristics, nanorods prove interesting for optical applications [1]. Nanorods can be used as nanoantennae and have been shown to be useful for many applications such as in enhancing light-emitter

Competing interests: The authors have declared that no competing interests exist.

interactions [4,5], high-resolution microscopy and spectroscopy [6], optical sensors [7–10], plasmonics in THz range [11], solar cells [12–18], and photocurrent generation [19].

Others have both computational and experimentally investigated plasmonic properties of various metal nanostructures [20] including gold nanowires [21], nanobars [22], nanorods [23]-[24], nanorod arrays [25], nanodiscs [25,26], gold dimers [27], triangular silver prisms [28], nanocuboids [29], nanostar [30] and hybrid or heterostructures [31,32]. These works show that plasmonic properties depend on size, shape, material, and dielectric environment [30,33]. Previous studies have investigated length [34], aspect ratio [35], polarization of incident light [36], and nanostructure fabrication method [37]. Various methods have been used to evaluate the plasmonic properties, such as discrete dipole approximation [38], quasistatic approximation [39], etc. While much work investigates the plasmonic properties in nanorods that have a circular cross-section, here we investigate the plasmonic properties of Au nanobars that have a rectangular cross-section and carefully examine the effects of their thicknesses using a finite element method. Importantly, we explore the differences between sharp-corner nanobars and more realistic round-corner nanobars in terms of the resonance wavelength and optical enhancement as the thickness is varied.

Methods

Computational analyses were performed on gold nanobars of constant length and width with different thicknesses using COMSOL simulations. The simulations are performed in three-dimensional space, where the length of the nanobar is 100 nm, the width is 60 nm, and the thickness varies from 8 nm to 60 nm. The geometries are chosen to represent nanobar structures that can be fabricated with electron beam lithography on a silicon substrate with a silicon dioxide layer. The substrate effect was approximated by an effective medium $n_{eff} = 1.25$ around the nanobar [40–43]. For gold, the optical properties are obtained from Johnson and Christy [44]. A normally incident light was directed onto the surface of the nanobar with the electric field polarized along either the longitudinal or transverse direction as shown in the insets of Fig 1. For the simulation, two types of rectangular nanobars, sharp-corner and round-corner, were investigated. The round-corner bars have a 15 nm fillet on the vertical edges. Absorption of the nanobars was calculated using the heat loss in the volume of the nanobars. The optical enhancement, defined as the ratio of the local electric field $\boldsymbol{E}$ to the incident electric field $\boldsymbol{E}_0$ squared (E^2/E_0^2), was studied since light intensity is proportional to the electric field squared. Around the sample, an integration space of radius 125 nm has been defined for the near-field region where most of the enhancement occurs. This integration space was used to calculate the optical enhancement of the nanobar.

Results and discussion

The absorption spectra of the nanobars was calculated for each thickness variation and is plotted in Fig 1 for both longitudinal (A) and transverse (B) incident polarizations. Each line on the plot indicates the spectrum of a single nanobar with a particular thickness. The plot shows that the absorption peak shifts toward blue as the thickness increases for both polarizations. For a given thickness, the large peak in the spectrum corresponds to the dipolar resonant plasmonic mode, and the smaller peaks at the lower wavelenghts are due to higher order modes. This is illustrated and discussed more later with our charge distribution calculations. These results are consistent with previous results on nanobars [29].

For the transverse polarization, the observed trend is same but the amplitude is reduced compared to the longitudinal polarization. The resonance peak value comparing the two polarizations for the same geometrical parameters gives different position. For longitudinal

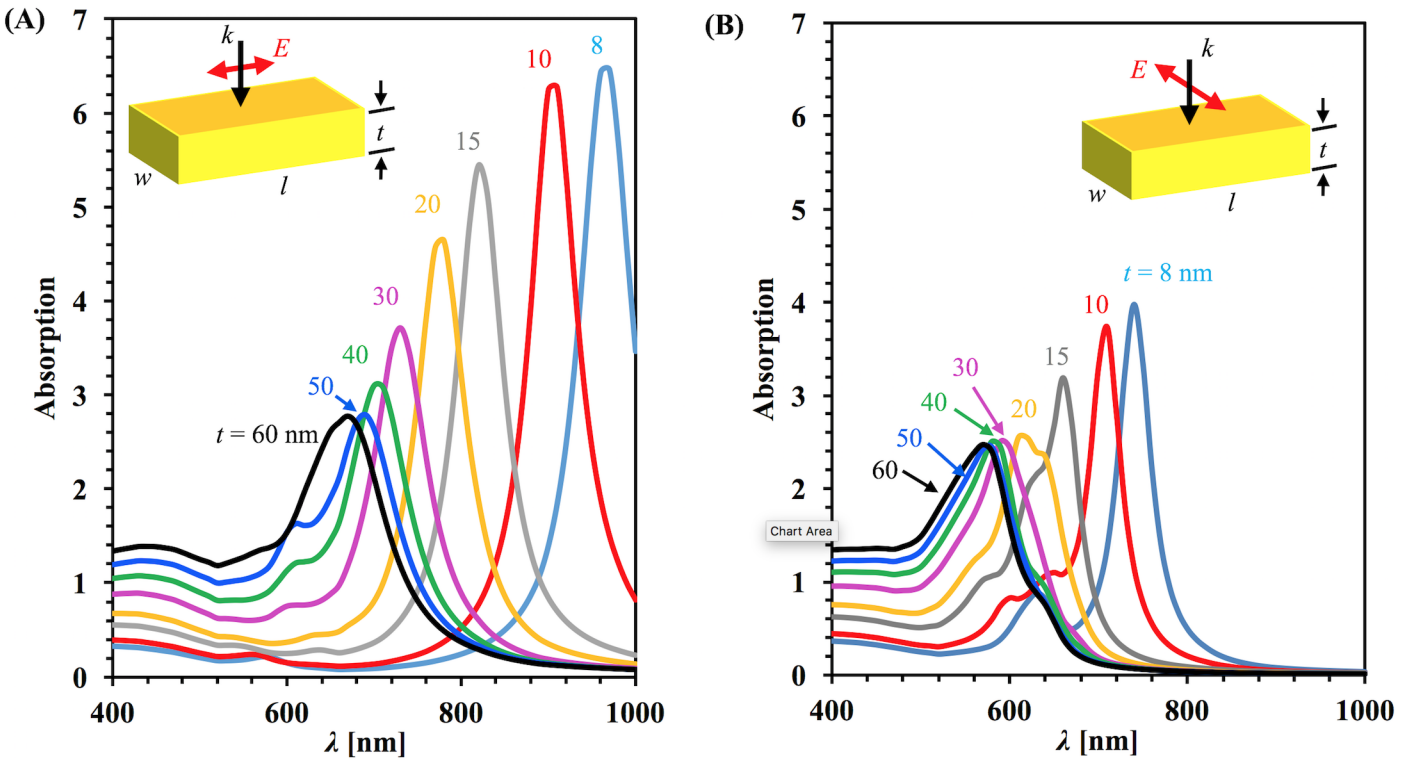

Fig 1. Calculated absorption spectrum. For the sharp-corner rectangular gold nanobar with different thickness (A) For longitudinal polarization and (B) for transverse polarization. In both cases light is normally incident. Insets show to top view of the nanobar with polarization direction.

https://doi.org/10.1371/journal.pone.0177463.g001

polarization, the resonance wavelength value is larger than for the transverse polarization because plasmonic response depends on the geometric length along which the electric field is polarized [45]. The full-width at half maximum of the spectrum also increases with increasing thickness.

Fig 2 shows the optical enhancement spectra for nanobars of constant length and width with different thicknesses for both longitudinal (A) and transverse (B) polarizations. Again the enhancement peak shifts towards blue with increasing thicknesses. Many studies looking at the length of the nanobars have found that increasing the length of the nanobars shifts the resonance peaks towards the red [4,24]. This difference arises due to the direction of the k-vector. When the k-vector is perpendicular to the dimension of interest, such as length, then the previous results hold true. For a k-vector parallel to the dimension of interest, the peaks blue-shift as thickness increases. For the same gold thickness, the peak resonance wavelength and normalized amplitude exhibit significant differences due to the different polarizations for both absorption and enhancement. For polarization along the long axis, electrons oscillate in a larger space, taking a longer time to oscillate, causing a lower frequency, and as a result the peak resonance wavelength is longer than polarization along the short axis of the nanobars [46].

The electric field distribution ($\boldsymbol{E/E_0}$) is shown at the resonant wavelength for each thickness for the sharp-corner and round-corner rectangular gold nanobars in Figs 3(A) and 4(A) respectively. The maximum amplitude of the electric field distribution at the resonant wavelength decreases as the thickness increases. This is due to the top and bottom plasmons decoupling for large thicknesses.

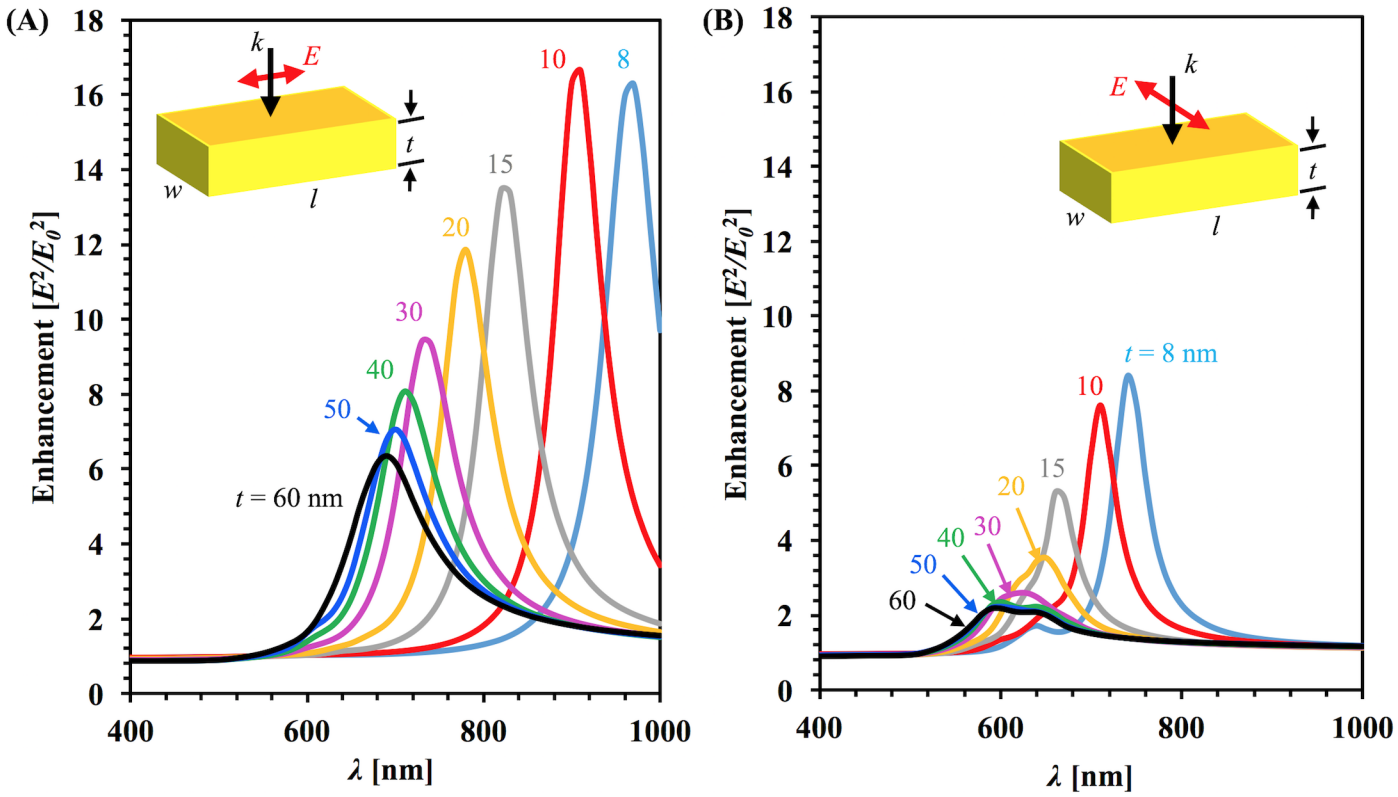

Fig 2. Calculated average enhancement spectrum. Spectrum was calculated in the integrated volume of the sharp-corner rectangular gold nanobar for normal light incidence in the effective medium (n_{eff} = 1.25) with different thickness for (A) longitudinal polarization (B) transverse polarization.

https://doi.org/10.1371/journal.pone.0177463.g002

Fig 5(A) shows the maximum electric field enhancement of sharp-corner and round-corner structures under longitudinal and transverse polarizations of incident light as a function of thickness. Maximum enhancement decreases with increasing thickness. The sharp-corner structures have a maximum enhancement that is between 3–18% greater than round-corner

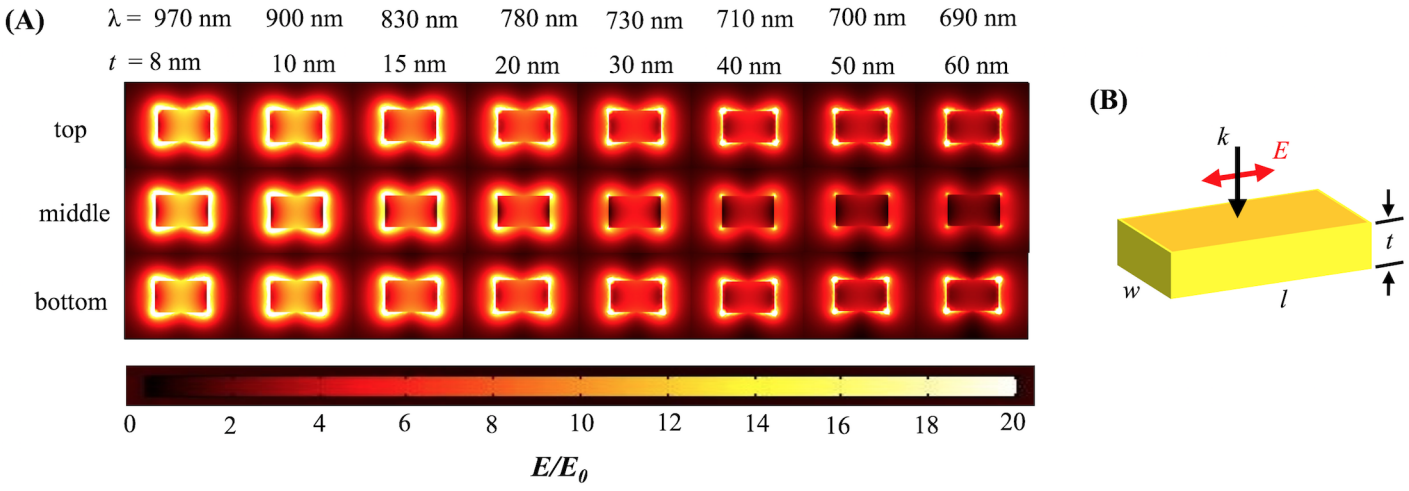

Fig 3. Electromagnetic field distributions for sharp-corner nanobar. (A) Field distribution for top, middle, and bottom surfaces at resonance wavelengths for sharp-corner Au nanobars of length 100 nm and width 60 nm for different thickness when polarization is aligned along the long axis and normal incidence. (B) Schematic of sharp-corner nanobar.

https://doi.org/10.1371/journal.pone.0177463.g003

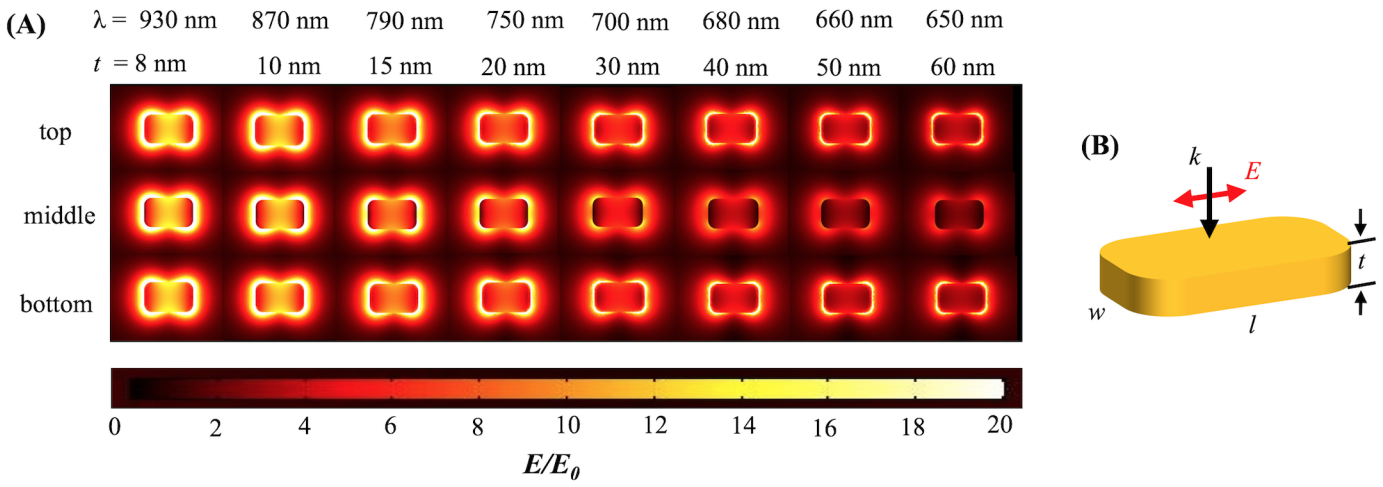

Fig 4. Electromagnetic field distributions for round-corner nanobar. (A) Field distribution for top, middle and bottom surfaces at resonance wavelengths for round-corner Au nanobars of length 100 nm and width 60 nm for different thickness when polarization along the long axis and normal incidence. (B) Schematic of round-corner nanobar.

https://doi.org/10.1371/journal.pone.0177463.g004

structures for longitudinal polarization with and average of a 12% increase, and the enhancement increase ranges from 10–46% with an average of 21% for transverse polarization. In practice, nanobars fabricated with lithography will have rounded corners due to the finite radius of the electron beam. For the longitudinal polarization, the maximum enhancement decreases

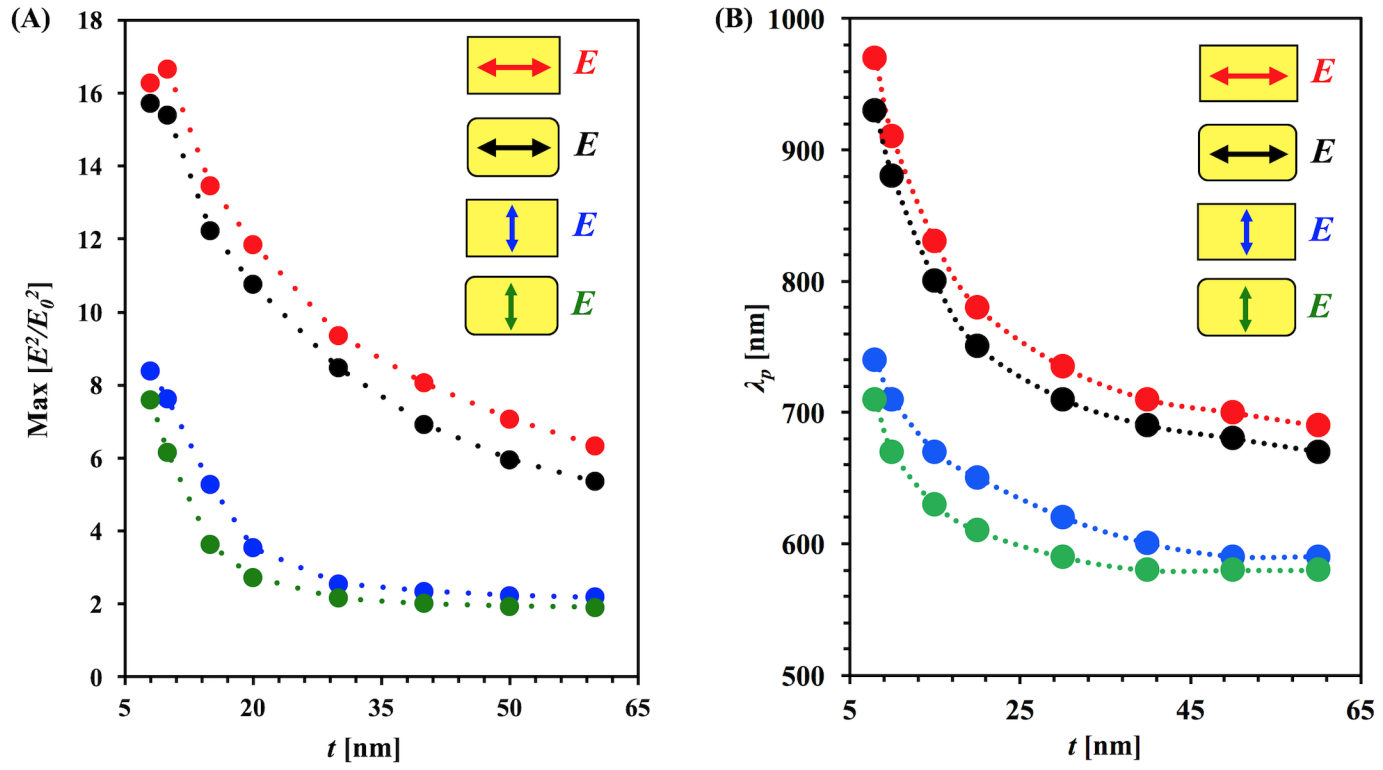

Fig 5. Dependance of maximum enhancement and peak resonance wavelength on thickness. (A) Normalized maximum enhancement [arb. unit] at resonant incident wavelength as a function of thickness for sharp-corner and round-corner nanobars for longitudinal and transverse polarization (B) Peak resonance wavelength as a function of thickness for both longitudinal and transverse polarization.

https://doi.org/10.1371/journal.pone.0177463.g005

quickly and tends toward a stable value at higher thickness. For transverse polarization for both shapes, the maximum enhancement decreases quickly up to 20 nm thickness; after that, the change becomes significantly less and eventually the maximum enhancement reaches a constant value. For large thicknesses, the plasmon modes are dominated by the dipole mode of the surface charges; those are well distributed on the surface of the nanoparticle. In this case, the surface charges are not strongly confined, creating only a weak enhancement. In case of small thicknesses, the resonance includes higher modes along with the dipole mode. The dipole mode's polarization source charges are well confined around the corners and edges of the nanobar, creating localized strong hot spots that generate strongly enhanced fields. The sharp corner nanobar accumulates more charges in the corners than round corner nanobars which makes a greater difference in the electric field enhancement. Additionally, increases in free electron density cause a blue shift of the surface plasmon resonance due to the enhanced restoring force [47].

Fig 5(B) shows the peak resonance wavelength for the enhancement spectrum as a function of thickness. As the thickness increases, the peak resonance wavelength shifts toward blue for both polarizations for both sharp-corner and round-corner nanobars. Additionally, the resonant wavelength for the round-corner structures is blue-shifted by 10 to 40 nm relative to the sharp corners. The nanobars with round corners have a reduced effective dimension along the side with the round corners which contributes to the blue-shift. Another contribution is due to the charge distribution; in round-corner nanobars, charges spread more than sharp-corner nanobars, which leads to a blue shift [48]. This is an important factor to consider when designing and tuning nanobars for plasmonic applications.

Fig 6 demonstrates the surface charge distributions for three different thicknesses for longitudinal polarization. Using Gauss's law (Eq 1) surface charge was calculated through the metal surface, S [49].

$$Q = n_{eff}^2 \cdot \varepsilon_0 \oiint (\boldsymbol{n} \cdot \boldsymbol{E}) dS = n_{eff}^2 \cdot \varepsilon_0 \oiint (\boldsymbol{n_x} \cdot \boldsymbol{E_x} + \boldsymbol{n_y} \cdot \boldsymbol{E_y} + \boldsymbol{n_z} \cdot \boldsymbol{E_z}) dS \quad (1)$$

Fig 6(A) shows the surface charge distribution for a nanobar with a thickness of 8 nm. At the resonance wavelength 580 nm the charge distribution forms a quadrupole while at 970 nm there is a dipole moment. Similar behavior was found for 20 nm and 50 nm thickness. These wavelengths reflect the two different peaks shown earlier in Fig 1. At the primary resonance wavelength, there is a dipolar distribution while at the shorter, lower intensity peak there is a quadrupolar distribution.

For small thickness, the dipole on the top surface and the dipole on the bottom surface are strongly coupled to each other and have a larger effective total charge. As the thickness increases, these dipoles begin to decouple and act more as separate dipoles. This causes a decrease in the total effective oscillating charge, thereby increasing the oscillation frequency, resulting in a blue shift. In addition, as the charges decouple, the higher order modes become more prominent. This change in relative intensities between modes, along with the primary resonant peak blue-shifting due to the higher orders, results in a broader spectral peak.

Fig 7(A) plots the full-width at half maximum (FWHM) as a function of resonance energy for each geometry. For absorption and enhancement, the figure shows nonlinear behavior with resonance energy. Fig 7(B) plots the FWHM of the broadening of the enhancement and absorption spectra as a function of thickness. For both cases, the plots show that FWHM generally increases with thickness; this is in part due to the superposition of the dipolar mode with higher order modes at lower wavelegnths.

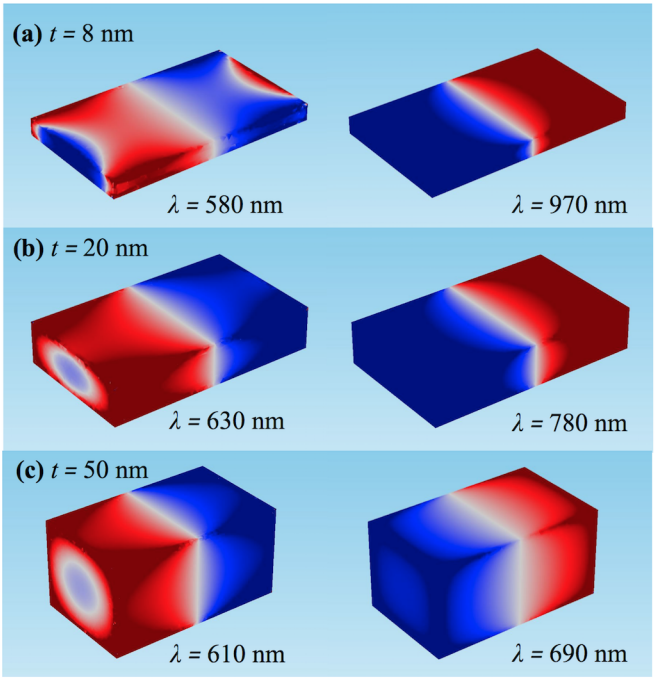

Fig 6. Surface charge distributions. At peak resonance wavelength when the thickness is (a) 8 nm (b) 20 nm and (c) 50 nm.

https://doi.org/10.1371/journal.pone.0177463.g006

The enhancement and absorption spectra broaden with the thickness of the structure. Fig 7 (A) shows an interesting result; when the thickness is changed, FWHM increases with the nanobar thickness. It shows a similar trend to that in Y-H Qiu et al. [23] where plasmon width was plotted as a function of longitudinal surface plasmon resonance (L-SPR) energy as the

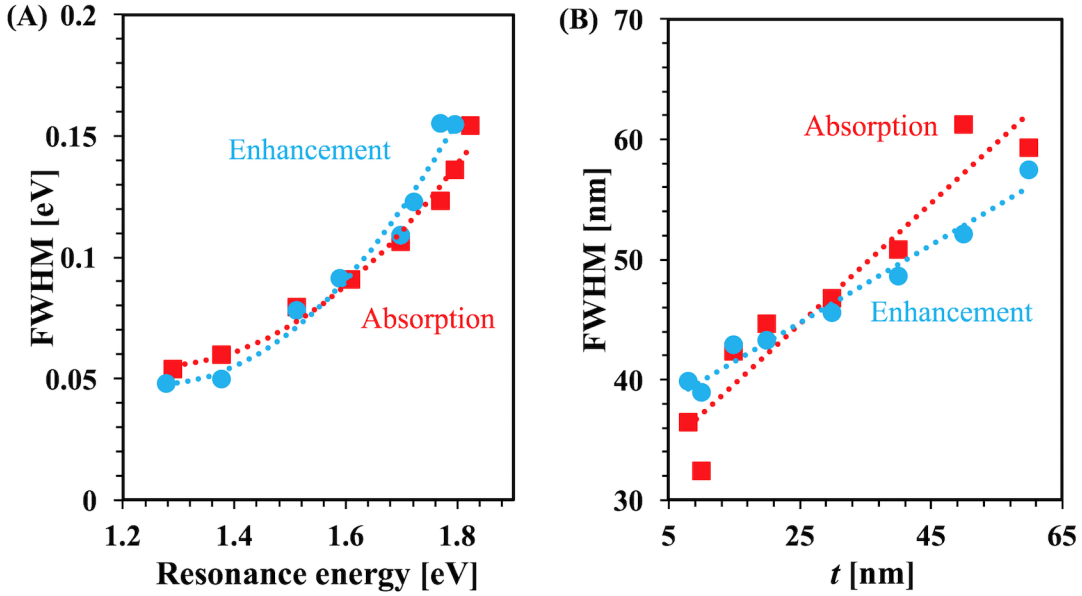

Fig 7. Resonance energy and thickness dependend FWHM. (A) Full width half maximum as a function of resonance energy (B) Full width half maximum as a function of thickness, where light incident normally.

https://doi.org/10.1371/journal.pone.0177463.g007

gold nanobar length was changed. This broadening is because of interband excitation induced damping [23]. In plasmon relaxation dynamics, a three-level system was introduced by Y-H Qiu et al. According to this system, a fixed frequency is used to excite the electron from ground state to the second excited state. A two-step process is used by electrons to go to the ground state; first, the electrons transition from second excited state to the first excited state then from first excited state to the ground state. From the second excited state to the first excited state, the electron goes through a process called electron-phonon relaxation, and from the first excited state to the ground state, the electron transitions with decay rate due to the phonon-phonon relaxation process.

Conclusion

In this study, plasmonic properties of gold nanobars with various thicknesses were computationally analyzed. Sharp-corner and round-corner rectangular nanobars were studied; comparisons of the peaks the spectra reveal that the round-corner nanobars shows an average of 30 nm shift to lower wavelength for the same size for both incident polariztations. Resonance peak wavelengths shifted toward blue for both absorption and enhancement spectra with increasing thicknesses due to decoupling of the charge dipoles on the top and bottom surface. As the thickness increases, the FWHM of the spectrum also increases due to the impact of higher order modes which have been visualized in our surface charge density distrubution calculations. The results reported here are significant for plasmonic structures fabricated with elelectron beam lithography since we investigate key fabrication parameters including thickness of the nanobars and round corners, a property of nanostructures fabricated with method.

Supporting information

S1 File. Data file for sharp corner structures.
(XLSX)

S2 File. Data file for rounded corner structures.
(XLSX)

Author Contributions

Conceptualization: PKG DTD DAF JBH.

Data curation: PKG DTD.

Formal analysis: PKG DTD JBH.

Funding acquisition: JBH.

Investigation: PKG DTD.

Methodology: PKG DTD JBH.

Project administration: JBH.

Resources: JBH.

Software: PKG DTD JBH.

Supervision: JBH.

Validation: PKG DTD JBH.

Visualization: PKG DTD JBH.

Writing – original draft: PKG.

Writing – review & editing: PKG DTD DAF JBH.

References

1. Sönnichsen C, Franzl T, Wilk T, von Plessen G, Feldmann J, Wilson O, et al. Drastic Reduction of Plasmon Damping in Gold Nanorods. Phys Rev Lett. 2002 Jan 31; 88(7):77402.
2. Kreibig U, Vollmer M. Optical Properties of Metal Clusters. Springer Science & Business Media; 2013. 552 p.
3. Wissert MD, Moosmann C, Ilin KS, Siegel M, Lemmer U, Eisler H-J. Gold nanoantenna resonance diagnostics via transversal particle plasmon luminescence. Opt Express. 2011 Feb 14; 19(4):3686. https://doi.org/10.1364/OE.19.003686 PMID: 21369194
4. Massa E, Maier SA, Giannini V. An analytical approach to light scattering from small cubic and rectangular cuboidal nanoantennas. New J Phys. 2013 Jun 10; 15(6):63013.
5. Dai H, Li M, Li Y, Yu H, Bai F, Ren X. Effective light trapping enhancement by plasmonic Ag nanoparticles on silicon pyramid surface. Opt Express. 2012 Jul 2; 20(S4):A502.
6. Farahani JN, Pohl DW, Eisler H-J, Hecht B. Single Quantum Dot Coupled to a Scanning Optical Antenna: A Tunable Superemitter. Phys Rev Lett. 2005 Jun 28; 95(1):17402.
7. Schuck PJ, Fromm DP, Sundaramurthy A, Kino GS, Moerner WE. Improving the Mismatch between Light and Nanoscale Objects with Gold Bowtie Nanoantennas. Phys Rev Lett. 2005 Jan 13; 94 (1):17402.
8. Mühlschlegel P, Eisler H-J, Martin OJF, Hecht B, Pohl DW. Resonant optical antennas. Science. 2005 Jun 10; 308(5728):1607–9. https://doi.org/10.1126/science.1111886 PMID: 15947182
9. Zhang S, Bao K, Halas NJ, Xu H, Nordlander P. Substrate-Induced Fano Resonances of a Plasmonic Nanocube: A Route to Increased-Sensitivity Localized Surface Plasmon Resonance Sensors Revealed. Nano Lett. 2011 Apr 13; 11(4):1657–63. https://doi.org/10.1021/nl200135r PMID: 21410217
10. Ozhikandathil J, Packirisamy M. Simulation and Implementation of a Morphology-Tuned Gold Nano-Islands Integrated Plasmonic Sensor. Sensors. 2014 Jun 13; 14(6):10497–513. https://doi.org/10.3390/s140610497 PMID: 24932868
11. Giannini V, Berrier A, Maier SA, Sánchez-Gil JA, Rivas JG. Scattering efficiency and near field enhancement of active semiconductor plasmonic antennas at terahertz frequencies. Opt Express. 2010 Feb 1; 18(3):2797–807. https://doi.org/10.1364/OE.18.002797 PMID: 20174108
12. Macpherson HA, Stoldt CR. Iron pyrite nanocubes: size and shape considerations for photovoltaic application. ACS Nano. 2012 Oct 23; 6(10):8940–9. https://doi.org/10.1021/nn3029502 PMID: 22978247
13. Derkacs D, Lim SH, Matheu P, Mar W, Yu ET. Improved performance of amorphous silicon solar cells via scattering from surface plasmon polaritons in nearby metallic nanoparticles. Appl Phys Lett. 2006 Aug 28; 89(9):93103.
14. Mokkapati S, Catchpole KR. Nanophotonic light trapping in solar cells. J Appl Phys. 2012 Nov 15; 112 (10):101101.
15. Li X, Hylton NP, Giannini V, Lee K-H, Ekins-Daukes NJ, Maier SA. Bridging electromagnetic and carrier transport calculations for three-dimensional modelling of plasmonic solar cells. Opt Express. 2011 Jul 4; 19 Suppl 4:A888–896.
16. Catchpole KR, Polman A. Plasmonic solar cells. Opt Express. 2008 Dec 22; 16(26):21793. PMID: 19104612
17. Ferry VE, Verschuuren MA, Li HBT, Verhagen E, Walters RJ, Schropp REI, et al. Light trapping in ultrathin plasmonic solar cells. Opt Express. 2010 Jun 21; 18(S2):A237.
18. Pillai S, Catchpole KR, Trupke T, Green MA. Surface plasmon enhanced silicon solar cells. J Appl Phys. 2007 May 1; 101(9):93105.
19. Abbey GP, Nusir AI, Manasreh O, Herzog JB. Structural characteristics of Au-GaAs nanostructures for increased plasmonic optical enhancement. Proc SPIE. 2016 Mar 15; 9758 0N.
20. Ekinci Y, Solak HH, Löffler JF. Plasmon resonances of aluminum nanoparticles and nanorods. J Appl Phys. 2008 Oct 15; 104(8):83107.
21. Giannini R, Hafner CV, Löffler JF. Scaling Behavior of Individual Nanoparticle Plasmon Resonances. J Phys Chem C. 2015 Mar 19; 119(11):6138–47.

22. Wiley BJ, Chen Y, McLellan JM, Xiong Y, Li Z-Y, Ginger D, et al. Synthesis and Optical Properties of Silver Nanobars and Nanorice. Nano Lett. 2007 Apr 1; 7(4):1032–6. https://doi.org/10.1021/nl070214f PMID: 17343425

23. Qiu Y-H, Nan F, Zhang Y-F, Wang J-H, He G-Y, Zhou L, et al. Size-dependent plasmon relaxation dynamics and saturable absorption in gold nanorods. J Phys Appl Phys. 2016; 49(18):185107.

24. Muskens OL, Giannini V, Sánchez-Gil JA, Gómez Rivas J. Optical scattering resonances of single and coupled dimer plasmonic nanoantennas. Opt Express. 2007; 15(26):17736. PMID: 19551070

25. Langhammer C, Kasemo B, Zorić I. Absorption and scattering of light by Pt, Pd, Ag, and Au nanodisks: Absolute cross sections and branching ratios. J Chem Phys. 2007; 126(19):194702. https://doi.org/10.1063/1.2734550 PMID: 17523823

26. Jain PK, El-Sayed MA. Plasmonic coupling in noble metal nanostructures. Chem Phys Lett. 2010 Mar 5; 487(4–6):153–64.

27. Wu J, Lu X, Zhu Q, Zhao J, Shen Q, Zhan L, et al. Angle-Resolved Plasmonic Properties of Single Gold Nanorod Dimers. Nano-Micro Lett. 2014 Sep 26; 6(4):372–80.

28. Kelly KL, Coronado E, Zhao LL, Schatz GC. The Optical Properties of Metal Nanoparticles: The Influence of Size, Shape, and Dielectric Environment. J Phys Chem B. 2003 Jan 1; 107(3):668–77.

29. Massa E, Maier SA, Giannini V. An analytical approach to light scattering from small cubic and rectangular cuboidal nanoantennas. New J Phys. 2013 Jun 10; 15(6):63013.

30. Shiohara A, Langer J, Polavarapu L, Liz-Marzán LM. Solution processed polydimethylsiloxane/gold nanostar flexible substrates for plasmonic sensing. Nanoscale. 2014 Jul 24; 6(16):9817–23. https://doi.org/10.1039/c4nr02648a PMID: 25027634

31. Polavarapu L, Mourdikoudis S, Pastoriza-Santos I, Pérez-Juste J. Nanocrystal engineering of noble metals and metal chalcogenides: controlling the morphology, composition and crystallinity. CrystEngComm. 2015 May 12; 17(20):3727–62.

32. Polavarapu L, Liz-Marzán LM. Growth and galvanic replacement of silver nanocubes in organic media. Nanoscale. 2013 May 3; 5(10):4355–61. https://doi.org/10.1039/c3nr01244a PMID: 23571840

33. Kelly KL, Coronado E, Zhao LL, Schatz GC. The Optical Properties of Metal Nanoparticles: The Influence of Size, Shape, and Dielectric Environment. J Phys Chem B. 2003 Jan 1; 107(3):668–77.

34. Muskens OL, Giannini V, Sánchez-Gil JA, Gómez Rivas J. Optical scattering resonances of single and coupled dimer plasmonic nanoantennas. Opt Express. 2007; 15(26):17736. PMID: 19551070

35. Fernández-López C, Polavarapu L, Solís DM, Taboada JM, Obelleiro F, Contreras-Cáceres R, et al. Gold Nanorod—pNIPAM Hybrids with Reversible Plasmon Coupling: Synthesis, Modeling, and SERS Properties. ACS Appl Mater Interfaces. 2015 Jun 17; 7(23):12530–8. https://doi.org/10.1021/am5087209 PMID: 25850108

36. Huang Y, Kim D-H. Dark-field microscopy studies of polarization-dependent plasmonic resonance of single gold nanorods: rainbow nanoparticles. Nanoscale. 2011; 3(8):3228. https://doi.org/10.1039/c1nr10336a PMID: 21698325

37. Shao L, Tao Y, Ruan Q, Wang J, Lin H-Q. Comparison of the plasmonic performances between lithographically fabricated and chemically grown gold nanorods. Phys Chem Chem Phys. 2015; 17(16):10861–70. https://doi.org/10.1039/c5cp00715a PMID: 25820223

38. Stefan Kooij E, Poelsema B. Shape and size effects in the optical properties of metallic nanorods. Phys Chem Chem Phys. 2006; 8(28):3349. https://doi.org/10.1039/b518389h PMID: 16835684

39. Wang F, Shen YR. General Properties of Local Plasmons in Metal Nanostructures. Phys Rev Lett. 2006 Nov 17; 97(20):206806. https://doi.org/10.1103/PhysRevLett.97.206806 PMID: 17155706

40. Saylor C, Novak E, Debu D, Herzog JB. Investigation of maximum optical enhancement in single gold nanowires and triple nanowire arrays. J Nanophotonics. 2015; 9(1):093053–093053.

41. Herzog JB, Knight MW, Li Y, Evans KM, Halas NJ, Natelson D. Dark Plasmons in Hot Spot Generation and Polarization in Interelectrode Nanoscale Junctions. Nano Lett. 2013 Mar 13; 13(3):1359–64. https://doi.org/10.1021/nl400363d PMID: 23398028

42. Herzog JB, Knight MW, Natelson D. Thermoplasmonics: Quantifying Plasmonic Heating in Single Nanowires. Nano Lett. 2014 Feb 12; 14(2):499–503. https://doi.org/10.1021/nl403510u PMID: 24382140

43. Choy TC. Effective Medium Theory: Principles and Applications. Oxford University Press; 2015. 257 p.

44. Johnson PB, Christy RW. Optical Constants of the Noble Metals. Phys Rev B. 1972 Dec 15; 6(12):4370–9.

45. Song M, Chen G, Liu Y, Wu E, wu B, Zeng H. Polarization properties of surface plasmon enhanced photoluminescence from a single Ag nanowire. Opt Express. 2012 Sep 24; 20(20):22290. https://doi.org/10.1364/OE.20.022290 PMID: 23037377

46. Knight MW, Liu L, Wang Y, Brown L, Mukherjee S, King NS, et al. Aluminum Plasmonic Nanoantennas. Nano Lett. 2012 Nov 14; 12(11):6000–4. https://doi.org/10.1021/nl303517v PMID: 23072330

47. Chen H, Shao L, Li Q, Wang J. Gold nanorods and their plasmonic properties. Chem Soc Rev. 2013; 42 (7):2679–724. https://doi.org/10.1039/c2cs35367a PMID: 23128995

48. Raziman TV, Martin OJF. Polarisation charges and scattering behaviour of realistically rounded plasmonic nanostructures. Opt Express. 2013 Sep 9; 21(18):21500–7. https://doi.org/10.1364/OE.21.021500 PMID: 24104025

49. Huang Y, Zhang X, Ringe E, Hou M, Ma L, Zhang Z. Tunable Lattice Coupling of Multipole Plasmon Modes and Near-Field Enhancement in Closely Spaced Gold Nanorod Arrays. Sci Rep. 2016 Mar 17; 6:23159. https://doi.org/10.1038/srep23159 PMID: 26983501